CIRP Annals Manufacturing Technology

Ultrashort pulsed laser drilling and surface structuring of microholes in stainless steels

L. Romoli[1], C.A.A. Rashed[1], G. Lovicu[1], G. Dini[1] (1), F. Tantussi[2], F. Fuso[2], M. Fiaschi[3]

[1] *Department of Civil and Industrial Engineering, University of Pisa, Italy*
[2] *Department of Physics, University of Pisa, Italy*
[3] *Continental Automotive Italy s.p.a., Italy*

Microholes for the production of gasoline direct injection nozzles were obtained by ultrashort pulsed laser machining in martensitic stainless steels. The inner surface analysis was carried out by a specifically conceived Scanning Probe Microscopy instrument and revealed the presence of periodic surface microstructures whose formation was studied as a function of process parameters (pulse energy, repetition rate, rotational speed, drilling strategy). Experiments demonstrated that geometrical features of the microstructures can be varied by a proper parameter selection and open the perspective for an optimized process enabling a reduction of coking accumulation during service life and a more effective atomization of the fuel jet.

Laser micro machining, Micro structure, Stainless steel

1. Introduction

The increasing concern for the environment protection has put the reduction of the pollutants and fuel consumption among the most important challenges for modern engines. Many of the improvements in this sense are related to the advances in fuel injection systems. The design of the internal nozzle flow is fundamental for the spray development and therefore in the air–fuel mixing and combustion processes.

In order to improve the atomization of the sprays and the mixing process, modern Gasoline Direct Injection (GDI) engines work at high injection pressures. The use of injection pressures up to 300 MPa brings the fuel at high velocity flowing through a contraction below the saturation pressure. Under these conditions the liquid starts to cavitate and a local change of state from liquid to vapour favours an increase in the spray cone angle, which is expected to improve the air–fuel mixing process [1].

Cavitating nozzles for GDI engines are conventionally produced by micro-Electric Discharge Machining (μ-EDM) with hole diameters of 150-200 μm and thickness of about 250-350 μm. Only recently ultrashort pulsed laser drilling has demonstrated to be an alternative technique enabling to work in dry environment with an even higher flexibility in changing the hole design. Smoother internal surfaces can be achieved in shorter processing times by fs-laser ablation respect to μ-EDM [2].

In addition to these benefits it is well known that ultrashort pulsed lasers, perpendicularly incident on workpiece, generate periodic patterns on the irradiated surfaces often referred to as Laser-Induced Periodic Surface Structure (LIPSS) [3]. The morphology of these structures varies with the material properties, the energy density used and the optical setup (polarization, incidence angle, etc.). The selection of appropriate process window enables to obtain oriented rippled structures whose height varies from 10 nm to 100 nm [4]. Such structures can be profitably used to control the wettability of a surface by enhancing or decreasing the hydrophobic properties of a material.

Objective of the present research is to combine a fast and precise laser drilling process of spray holes with the generation of a rippled pattern on the internal surface. This is extremely challenging for automotive applications since the structuring technique may lead to a remarkable reduction of coking deposition and avoid the risk of nozzle clogging as well. Moreover, tailor-designed periodic nanoripples on the hole inner surface can have a significant impact on fuel jet breaking with a consequent enhancement of spray atomization. Controlling the main features of the rippled pattern (e.g., spacing, orientation) requires designing of specific drilling processes, with possible differences with respect to commonly used percussion or trepanning techniques [5]. Conventional trepanning showed significant limits on the quality of the edges due to deposition of expelled material out of the circular groove.

2. Fundamentals of LIPSS formation

The ripples exhibit complex morphology sharing many similarities with other self-organized patterns originating from instabilities, such as aeolian sand dunes or ripples produced by ion-beam sputtering. In case of linearly polarized laser beams, the orientation is found to be perpendicular to the light polarization with a periodicity often smaller than the laser wavelength [6]. The periodicity has a correlation with the local intensity of the electromagnetic field transferred to the workpiece and with the boundary conditions at the material interface (e.g. type of gas) [7]. The microscopic mechanism of ripples formation is still under discussion: it is here assumed that excitation and subsequent ablation of target material by ultra-short laser pulses induce a state of extreme non-equilibrium of the surface [8]. The instability relaxes on a very short time scale through two competing processes, namely surface roughening due to

desorption (identified, with general acceptance, to be Coulomb and/or phase explosion) and surface smoothing due to diffusion. In fact for ultra-short laser pulses even if the energy transfer from incident beam to the lattice occurs via multiphoton excitation of the electronic system, there is a diffusive energy transport by hot electrons as long as there is no thermal equilibrium between electrons and phonons. The resulting electron thermal diffusion length is a key quantity for laser material interaction, determining a positively charged surface layer in a few picoseconds. Such surface ionization results in electrostatic instability and, thus, in Coulomb emission of positive charges. After this, the surface instability is even greater: surface erosion by ablation is in dynamic competition with surface smoothing by diffusion. Far from thermal equilibrium, the local state of the material is neither crystalline nor amorphous or liquid. More likely, it can be considered a "soft" state of the material [9]. The result of this instability relaxation is the self-organized formation of quasi-regular surface structures under the driving action of the absorbed electromagnetic field and the related optical interference effects responsible for the formation of the quasi regular patterns.

3. Experimental

Experiments were carried out on real injector components in order to assess the feasibility of the proposed drilling technique in a real production environment. GDI nozzles are commonly obtained in AISI 440C to combine good resistance to corrosion with wear resistance. This is because the hertzian contact with the internal spherical valve regulates the fuel spray cycle, as depicted in fig. 1 (a) and (b). Cylindrical spray holes with a diameter of 180 μm were laser drilled starting from the bottom surface of counterbores previously micromilled. The drilled thickness was 250 μm, lower than the laser Rayleigh distance. A 800 fs chirped pulse laser (λ=1552 nm) with a maximum average power of 5 W (50 μJ at 100 kHz) was used for the experiments. The laser beam was circularly polarized by an adjustable quarter wave plate to avoid roundness defects due to an uneven absorption of the p- and s- components of the electromagnetic field, parallel and orthogonal to the incidence plane on the inner surface [10], respectively. The beam was focused on the counterbore flat surface to a minimum spot size of 25 μm, with a nearly Gaussian energy distribution.

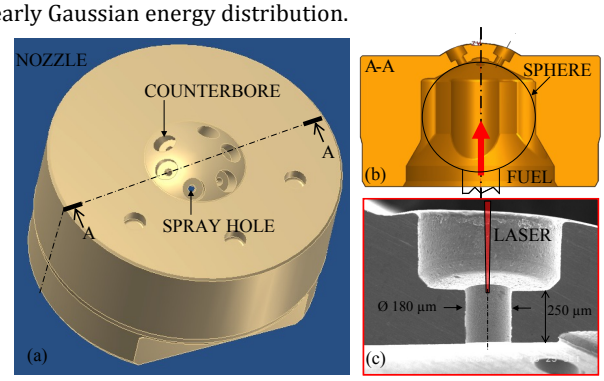

Fig. 1. (a) 3D view of a GDI nozzle: spray hole are drilled concentrically with the counterbores; (b) nozzle section: cone-sphere contact and fuel direction; (c) laser drilling direction and cylindrical hole geometry achieved at the end of the drilling process.

A five axes controlled stage was used to place the counterbore flat surfaces at the correct focal distance, normally to the beam axis. As specified in the following, the drilling strategy foresees the attainment of a tapered pre-hole followed by a final circular shaping. The beam was guided in circular drilling trajectories by a galvo-head (75 mm/s maximum tangential speed). Helium was used as assist gas (0.7 MPa) to shield the occurrence of plasma and to convey the ablated particles towards a suction probe placed under the nozzle.

Drilled microholes were cross sectioned at the center after measuring the hole taper by optical stereomicroscope. The inner walls were firstly inspected by scanning electron microscope (SEM) to verify the presence of LIPSS. Then a Shear Force Microscope (SHFM) tested in a previous research [2] was used to acquire topography maps of the inner walls. From these maps it was possible to measure the ripple average height and to derive inclination and periodicity of the surface pattern.

4. Drilling method for ordering internal ripples

The strong correlation between polarization direction and ripples orientation suggests the absorbed electromagnetic field vector into the sidewall to be the main control parameter for the self-arrangement of the surface "soft" state. Elliptical polarization at normal incidence (θ_i=0°) generates LIPSS elongated perpendicularly to the direction of the strong field (major axis of the ellipse) [9]. Conversely, circular polarization does not lead to LIPSS formation unless large θ_i are used. This is because the strong anisotropy in absorption of the p- and s- light components

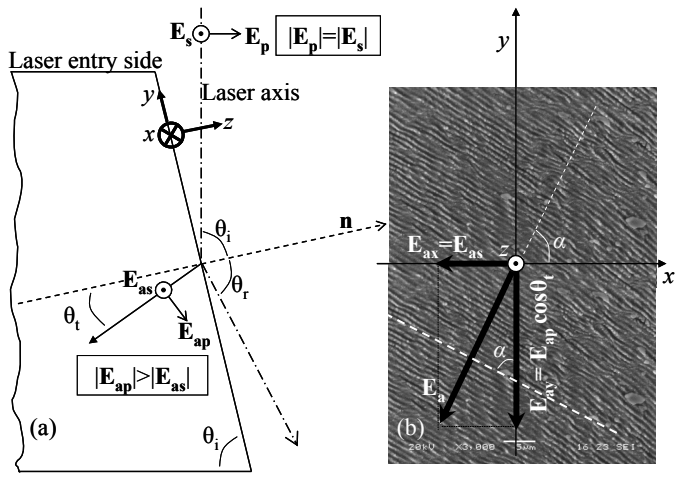

at grazing incidence produces an anisotropy in the electromagnetic field absorbed by the material, resulting in conditions similar to those experienced in [9]. The phenomenon is sketched in fig. 2: the tapered sidewall occurring in the pre-hole processing generates uneven absorption of circular polarization resulting in an effective field $\boldsymbol{E_a}$ oriented along a direction forming an angle α with respect to the x-axis.

Fig. 2. (a) Plane of incidence cross-sectioning the tapered pre-hole. It shows how to induce an asymmetry of the absorbed field; (b) absorbed field vector on the sidewall $\boldsymbol{E_a}$ over a SEM image of LIPSS with perpendicular orientation respect to the vector. SE CAMBI ALFA in BETA: the measured LIPSS angle β is equal to the angle α defining the direction of the absorbed field for geometrical reasons.

Ripples are consequently supposed to grow perpendicularly to the absorbed field direction [9]. In a simplified model [11], α can be related to θ_i and to the material properties starting from

$$\cos\theta_t = \frac{\sqrt{n^2 - \sin\theta_i}}{n} \qquad (1).$$

Where, θ_t is the refraction angle (see fig. 2 (a)) and n the refractive index of the material. Following an approach based on

the Fresnel laws [11], the relative amplitude of the x and y components of the absorbed electric field projected onto the sidewall surface, $\boldsymbol{E_{ax}}$ and $\boldsymbol{E_{ay}}$, can be determined. Finally, the angle α can be estimated by

$$\alpha = \arctan\left(\frac{E_{ay}}{E_{ax}}\right) \qquad (2).$$

Fig. 3 reports the results of the α calculation as a function of θ_i where the real part of n and the extinction coefficient k of the complex index of refraction, both entering into the calculation, were estimated 3.6 and 5.6 respectively, weighting the optical properties of the elements composing the used steel in the near IR, as found in the literature [12]. In the present research the polarization of the laser beam was kept constant, while other process parameters were modified in order to assess their role in LIPSS formation.

Fig. 3. Theoretical angle α of the absorbed field vector $\boldsymbol{E_a}$ with respect to x axis as a function of the angle of incidence of the beam on the sidewall.

Assumed that LIPSS are generated at the ultimate laser passes on the sidewall, a drilling procedure enabling the adjustment of surface pattern by controlling the taper angle of the pre-hole, ruling the angle of incidence (see fig. 2), can be then hypothesized. Subdividing the drilling procedure in three steps, as specified in the following, may lead to an increase in quality and in sharpness of the ablated edges and also in the control of the surface pattern.

1. Cylindrical through hole of 50-60 μm diameter obtained by a circular trepanning (fixed trajectory radius 17.5 μm). An internal core of 10 μm is indirectly ablated by energy diffusion. For passing through the material 60 turns are performed with 50 μJ pulses deployed at 100 kHz and 50mm/s tangential speed. This pilot hole has a rough aspect but allows helium to penetrate inside and better evacuate metal vapours.
2. Enlargement phase obtained with a spiral trajectory, at constant tangential speed of 50 mm/s, up to the nominal diameter (final trajectory radius 77.5 μm) with number of passes ranging between 50-100. Pulse energy adopted is 50 μJ at 100 kHz. It can be considered more appropriately a microcutting phase bringing to the expected tapered pre-hole for the generation of ordered LIPSS, as described above.
3. Cylindrical spray-hole is obtained by 50 additional turns at the final trajectory radius. The tapered exit of the hole is removed without enlarging the entry side. LIPSS are supposed to acquire their final structure in this phase evolving from the inclined surface created in the step two. Pulse energy (10-50 μJ), repetition rate (12.5-100 kHz) and tangential speed (10-75 mm/s) are varied to study their influence on the direction, period and size of the sidewall pattern.

5. Results and discussion

A typical cross section of spray-hole is shown in fig. 4: LIPSS structure was analyzed in three zones of the sidewall corresponding to the entrance of the laser, the center and the exit.

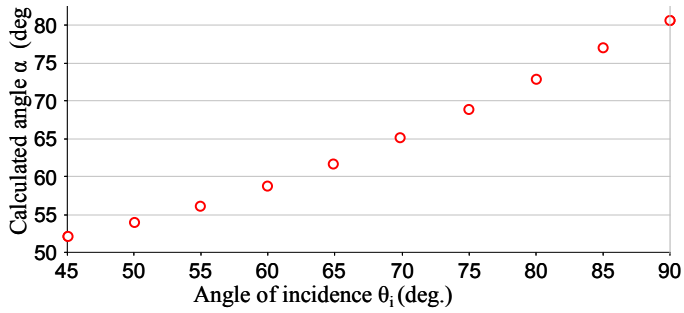

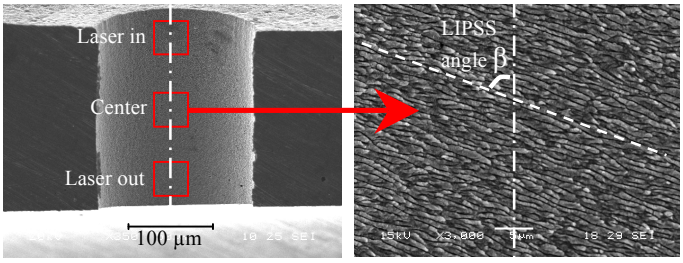

Fig. 4. SEM view of a spray-hole cross section and a detail of the sidewall showing LIPSS inclined respect to the hole axis by a measured angle β.

Geometrical features of the pattern were acquired in the three zones to verify the uniformity of the texturing process at increasing the drilled thickness. Maps (50μm x 50μm) acquired by the SHFM were used to derive the inclination of the LIPSS direction with respect to the hole axis using a self correlation procedure, as reported in fig. 5.

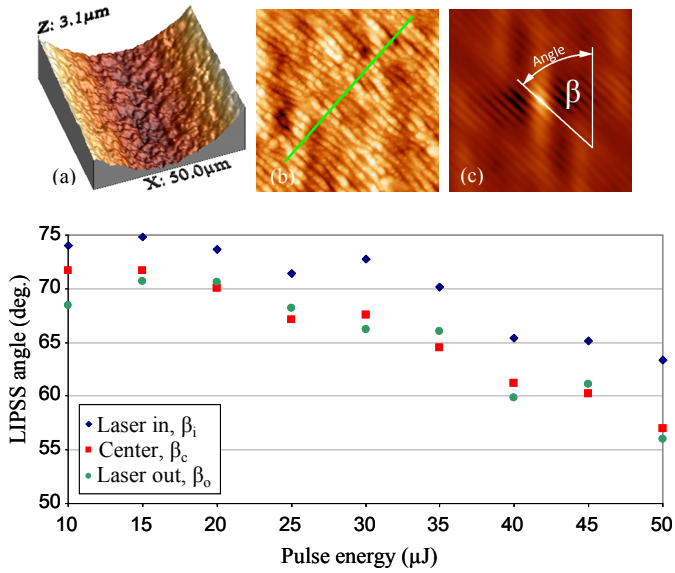

Fig. 5. (a) Typical 3D view of the acquired maps; (b) top view of the filtered map with visible LIPSS (hole curvature removed). The green segment represents the direction of a line profile analysis. (c) Self-correlation map used to derive the angle β..

Experiments showed that increasing the number of turns in the pre-hole enlargement step 2 varies θ_i almost linearly from 50° to 85°. The corresponding range in the LIPSS angle β is 53°-75° which is in well agreement with the theoretical expectations (see, e.g. fig. 3). Remarkably, LIPSS angle measured at the laser entrance zone (β_i) is higher than in the other regions, where inclination is almost constant. This can be explained with the hole tapering at the beginning of step 3, leading to larger θ_i values in the laser entrance region. Obviously the smaller the LIPSS angle β the smaller the inclination respect to the fuel jet, that is expected to make the cleaning of the sidewall surface much easier.

Results obtained increasing pulse energy in step 3 (at 100 kHz and speed 50 mm/s) are reported in fig. 6. Every point in the graph is the averaged value of three different measurements.

Fig. 6. LIPSS angle β vs. pulse energy for the three zones measured. Indexes of β (i, c , o) are referred to the tree zones reported in fig.4 (a).

LIPSS angle decreases slightly with increasing pulse energy: this can be linked to the higher quantity of material brought in the soft state by a larger amount of energy. Thermal diffusion length increases as well and a thicker layer is rearranged by the absorbed field. The pattern generated at the highest values in the investigated range shows shorter and less regular structures. LIPSS tend to bifurcate and to cross link each other, which does not correspond to the intended purpose of producing microstructures aimed at preventing coking deposition. Conversely pulses of 10-20 μJ do not generate a cylindrical hole after 50 turns, requiring additional drilling time, since the energy density *ED* supplied to the material (ratio between averaged power P_{avg} tangential speed *v* and spot diameter $Ø_{spot}$) decreases down to 0.8 J/mm²:

$$ED = \frac{P_{avg}}{v\phi_{spot}} = \frac{E_p f}{v\phi_{spot}} \quad (3).$$

Increasing repetition rate (at 50 μJ and 50 mm/s) shows an opposite behaviour leading to an increase of LIPSS angle (fig. 7). Especially, results obtained at 12.5 kHz shows an interesting pattern owing to its smaller inclination to the hole axis, more favourable to the evacuation of particles and coking deposition.

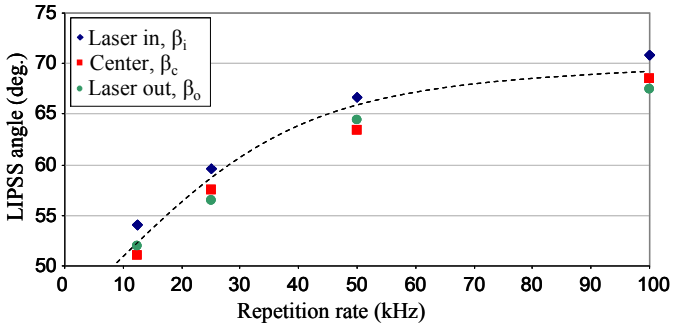

Fig. 7. LIPSS angle β vs. repetition rate for the three zones measured. The dashed line is a guide to show the trend.

LIPSS periodicity is the second important feature of the surface pattern: the higher the ripple spacing the easier the evacuation of residual particles and coking. Averaged crest-to-crest distance was measured by a Fourier transform analysis of the height profile along a sampling line perpendicular to the LIPSS

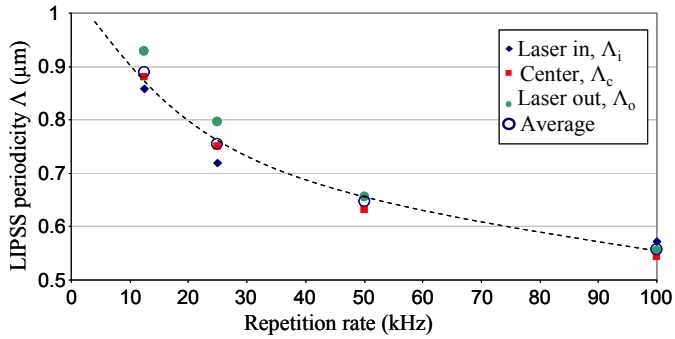

orientation (green line in fig. 5 (b)). The LIPSS periodicity Λ was found almost constant irrespective of the pulse energy adopted with an average value of 650 nm and a relative standard deviation of 0.02. On the contrary, a remarkable dependence was found as a function of the repetition rate (see fig. 8): the spacing at *f* =100 kHz was almost one half that at small repetition rate. From this observation it is possible to conclude that the time between two pulses has an influence on the developing texture. The longer time (80 μs) causes a coarser ripple size.

Fig. 8. LIPSS periodicity Λ vs. repetition rate for the three zones measured. The dashed line is a guide to show the trend.

Changing tangential speed has also some influence on LIPSS orientation and periodicity. Increasing *v*, pulse overlap and *ED* are lowered resulting in more elongated and spaced surface features. SHFM was used to measure the height profile of the generated LIPSS: data of root-mean-square surface roughness R_q were acquired perpendicularly to LIPSS orientation. R_q is about 100-120 nm for tangential speed in the range 10-40 mm/s even though the resulting *ED* (20-5 J/mm²) is high enough to melt the LIPSS crests together in an extremely disordered ripple pattern which makes the evacuation of particles almost impossible (fig. 9 (a)). Conversely the combination of *f*=12.5 kHz with *v*=75 mm/s even at the highest pulse energy (50 μJ) results in long and well spaced (~1μm) series of 50° orientated ripples, having an average height of 150 nm, as shown in fig. 9 (b). The much lower *ED* input (0.3 J/mm²) avoids secondary phenomena of ripple cross-linking leading to a disordered surface pattern. Anyhow the lack of *ED* to obtain a cylindrical hole has to be compensated by additional 50 turns (100 total turns for the step 3) at the final trajectory radius. These multiple passes do not vary the generated surface patterns being the time between 2 turns (10ms) several order of magnitude higher than the time for self-rearrangement of the surface under the action of the absorbed field.

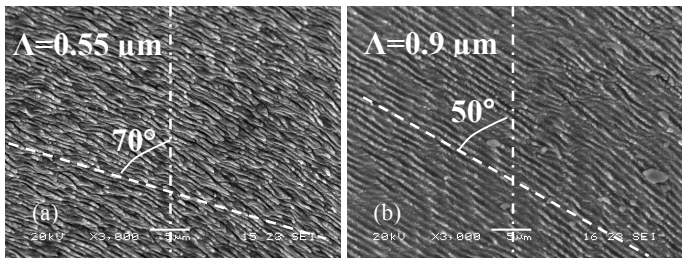

Fig. 9. E_p= 50 μJ: (a) entangled pattern obtained at 100 kHz and 25 mm/s; (b) well ordered pattern obtained at 12.5 kHz and 75 mm/s.

6. Conclusions

A 3-steps method for laser drilling cylindrical spray holes was proposed with the aim of generating the self-organized rippled pattern under the action of the absorbed electromagnetic field. The resulting drilling technique is able to attain the expected cylindrical shape within the process time of 2.5 s with respect to the 10.5 s of conventional μ-EDM. It enables as well to obtain a microstructuring of the inner hole surface with geometrical features depending on the process parameters. In particular, the proposed selection of parameters can represent a possible solution to the trade-off between process time and optimized surface structuring. First analysis on the drilled spray holes by high speed camera imaging of the spray development have shown improvements in the atomization effects considering that the averaged droplet size was found to decrease of about 10% respect to conventional laser trepanned holes while spray cone angle increased more than 20%. Cross sectional inspection of spray hole on injectors used for 50 h on a test GDI engine, revealed that coking is not covering the entire inner wall, as for μ -EDM processed injector nozzles.

References

[1] Z. He, W. Zhong, Q. Wang, Z. Jiang, Z. Shao (2013) Effect of nozzle geometrical and dynamic factors on cavitating and turbulent flow in a diesel multi-hole injector nozzle, *International Journal of Thermal Sciences* 70 pp. 132-143.

[2] L. Romoli, C.A.A. Rashed, M. Fiaschi (2014) Experimental characterization of the inner surface in micro-drilling of spray holes: a comparison between ultrashort pulsed laser and EDM, *Optics & Laser Technology* 56 pp. 35-42.

[3] M.N.W. Groenendijk, J. Meijer (2006) Surface microstructures obtained by

femtosecond laser pulses, *CIRP Annals - Manufacturing Technology* 55 pp. 183–186.

[4] L. Li, M. Hong, M. Schmidt, M. Zhong, A. Malshe, A.J. Huis in'tVeld, V. Kovalenko (2011) Laser nano-manufacturing – State of the art and challenges, *CIRP Annals - Manufacturing Technology* 60 pp. 735–755.

[5] K.H. Leitz, B. Redlingshöfer, Y. Reg, A. Otto, M. Schmidt (2011) Metal ablation with short and ultrashort laser pulses, *Physics Procedia* 12 pp. 230-238.

[6] G.R.B.E. Römer, A.J. Huis in't Veld, J. Meijer, M.N.W. Groenendijk (2009) On the formation of laser induced self-organizing nanostructures, *CIRP Annals - Manufacturing Technology* 58 pp. 201–204.

[7] W. Kautek, P. Rudolph, G. Daminelli, J. Krüger (2005) Physico-chemical aspects of femtosecond-pulse-laser-induced surface nanostructures, *Applied Physics A* 81 pp. 65-70.

[8] C. Wang, H. Huo, M. Johnson. M. Shen, E. Mazur (2010) The thresholds of surface nano-/micro-morphology modifications with femtosecond laser pulse irradiations, *Nanotechnology* 21 075304.

[9] J. Reif, O. Varlamova, F. Costache (2008) Femtosecond laser induced nanostructure formation: self-organization control parameters, *Applied Physics A* 92 pp. 1019–1024.

[10] S. Nolte, C. Momma, G. Kamlage, A. Ostendorf, C. Fallnich, F. von Alvensleben, H. Welling (1999) Polarization effects in ultrashort-pulse laser drilling, *Applied Physics A* 68 pp. 563–567.

[11] K.X. Pham, R. Tanabe, Y. Ito (2013) Laser-induced periodic surface structure formed on the sidewalls of microholes trepanned by femtosecond laser, *Applied Physics A* 112 pp. 485-493.

[12] M.A. Ordal, R.J. Bell, R.W. Alexander Jr., L.L. Long, M.R. Querry (1985) Optical Properties of fourteen metals in the infrared and far infrared, *Applied Optics* 24 pp. 4493-4499.